*Journal of Sound and Vibration* (2002) **251**(5), 823–846
doi:10.1006/jsvi.2001.4013, available online at http://www.idealibrary.com on IDEAL®

# ANALYSIS OF THE PERIODIC PRESSURE FLUCTUATIONS INDUCED BY FLOW OVER A CAVITY

H. KOOK

*Graduate School of Automotive Engineering, Kookmin University*, 861-1 *Chongnung-dong, Songbuk-gu, Seoul* 136-702, *Korea. E-mail: kook@kmu.kookmin.ac.kr*

AND

L. MONGEAU

*Ray W. Herrick Laboratories, School of Mechanical Engineering, Purdue University, West Lafayette, IN* 47907-1077, *U.S.A.*

(*Received* 31 *August* 2000, *and in final form* 10 *July* 2001)

Subsonic flows over Helmholtz resonators often cause strong periodic pressure fluctuations inside the resonators over a range of outer flow velocities. The flow-excitation mechanism is known to be governed by both the shedding of discrete vortices within the shear layer over the orifice and the acoustic response of the cavity. This self-sustained oscillation phenomenon is often analyzed by using a feedback loop model where the flow excitation and the acoustic response of the resonator are approximately modelled as a forward gain function and as a backward gain function respectively. In the present work, a similar approach was followed and a new forward gain function was derived based on the concept of "vortex sound" to model the flow excitation. The formulation combined this forward gain function with a backward gain function from previous work, within the framework of the feedback loop analysis. The approximate method allowed the frequency and the relative amplitude of the cavity pressure fluctuations to be predicted for a range of flow velocities. In addition, the extended Nyquist stability criterion was used to estimate the onset and the termination velocities of the first two modes of the shear layer flow oscillations. Experimental data were obtained using a rigid-walled cavity in a low-speed wind tunnel. The results showed that the model predictions were in reasonably good agreement with the experimental data.



## 1. INTRODUCTION

Cavities exposed to boundary layers and/or shear layers are often acoustically excited by outer flows over specific ranges of flow velocities. Instances of self-sustained and flow-excited resonance occur for many engineering applications such as for vehicles with open sunroofs [1], for pipelines with closed side branches [2], for aircraft landing gears [3]. Since the noise and vibrations that emanate from the flow-excited acoustic resonance of cavities are usually unwanted, many researchers have investigated the phenomenon in order to prevent it.

Many of the models previously proposed for this problem analyzed the instability of the shear layer based on stability theory where small wavelike disturbances of shear layers are analyzed by using a linear approximation [4–8]. The shear layer's lateral motion (i.e., motion in the direction perpendicular to the free stream flow direction) obtained by using linear stability theory can be expressed by a sinusoidal function with exponentially

0022-460X/02/$35.00 

increasing amplitude with the distance in the streamwise direction. Since the amplitude of the shear layer's fluctuations is predicted to grow unrealistically large at the downstream edge by linear stability theory, only the predicted phase information is useful subsequent analysis. In the models that use linear stability theory, the shear layer's periodic, lateral displacement over the cavity orifice is identified as the aerodynamically induced acoustic source. However, one limitation of linear stability theory is that it is not appropriate in the case of flows where the shear layer is rolled-up into discrete vortical structures [2].

Another method to analyze the shear layer's instability is the so-called "vortex-sound" theory [9, 10]. Vortex sound theory describes how sound can be induced by convection of discrete vortices. Bruggeman and his colleagues [2] used vortex sound theory for the problem of flow-excited cavities. In their work, the lift force due to the convection of discrete vortices over the orifice was interpreted as the acoustic source. Vortex sound theory was considered to be more appropriate to describe the acoustic sources for flows where the shear layer's disturbance cannot be represented by small wavelike motion. To predict the amplitudes and the frequencies of the pressure oscillations with the cavity (in this case, a side-branch resonator), an inhomogeneous convected wave equation with a source term related to vortex convection was solved using a Green's function method.

In many other models, most of which are based on linear stability theory, a feedback loop analysis [11–15] has been preferred to predict the amplitudes and the frequencies of the pressure within the cavity rather than the Green's function method. In a feedback loop model, the response of the flow-excited cavity system is considered to be given in the frequency domain by the product of the forward and the backward gain functions. The forward gain function represents the response of the flow instability to a sinusoidal acoustic input, while the backward gain function represents the acoustic response of the cavity resonator to a sinusoidal excitation. Once the two gain functions are modelled appropriately, the feedback loop analysis offers many advantages. It can readily be integrated in a design optimization scheme since the feedback loop method requires little computational time. A simple stability analysis that yields the onset and termination velocities of resonance can also be performed.

In the present study, an analytical model is proposed in the form of a feedback loop for a convenient description of resonator systems excited by low Mach number flows. Vortex sound theory is introduced to model of the forward gain function to overcome the limitations imposed by linear stability theory. Since the amplitude information predicted by the linear stability theory is not reliable, the amplitude gain of the forward gain function has been separately modelled based on an empirical scaling law, while the phase response of the forward gain function is obtained from the sinusoidal expression of the shear layer's displacement. However, it will be shown in later sections that the mathematical derivation procedures for both the phase response and the amplitude gain of the forward gain function can be unified by introducing vortex sound theory.

The derivation of the model also relied on the work of Nelson and his colleagues [16, 17] for the understanding of the basic excitation mechanism. After a new feedback loop model for the description of the flow-excited cavity systems is proposed, a stability analysis based on Nyquist stability criterion is described within the framework of the feedback loop model developed in the present work. The stability analysis allowed the prediction of the onset and termination velocities of resonance. It has rarely been attempted in previous studies.

## 2. FEEDBACK LOOP ANALYSIS AND THE BACKWARD GAIN FUNCTION

When a cavity resonator is excited by flow, the instantaneous total flow velocity, $\mathbf{v}$, over the cavity orifice can be decomposed into a purely vortical flow field and a potential flow field [17], i.e.,

$$\mathbf{v} = \bar{\mathbf{v}}_v + \mathbf{v}'_v + \nabla\bar{\phi} + \nabla\phi', \tag{1}$$

where $\mathbf{v}_v$ and $\nabla\phi$ represent the vortical flow field and the potential flow field, respectively, the overbar denotes a time average and the prime denotes the fluctuating component of the velocity field. Note that the acoustic flow is the unsteady part of the potential flow, which is denoted by $\nabla\phi'$ in equation (1). The sum of the first three terms on the right-hand side of equation (1) thus represents the remaining aerodynamic (or hydrodynamic) flow field.

It is known that the acoustic flow field and the aerodynamic flow field strongly interact with each other at a resonance condition. For instance, the acoustic flow velocity near the upstream edge of the cavity orifice determines the timing of a vortex shedding at the upstream edge and is involved in the vortex rolling-up process when shed vortices convect downstream. The aerodynamic flow field also influences the acoustic flow field: energy is transferred from the former to the latter flow field for specific conditions. For more detailed physics of interaction between the two flow fields, see references, for instance, references [17, 18].

In the feedback loop analysis of the flow-excited cavity system, each of the fluctuating acoustic and the aerodynamic flow velocity fields is approximated by the complex acoustic volume velocity, $\hat{q}_r$, and the complex aerodynamic volume velocity, $\hat{q}_o$ respectively. Both volume velocities are taken to be positive in the direction pointing into the cavity. Then, the controlling and controlled relationship between the two flows in a flow-excited system can be described by using a feedback loop as shown in Figure 1. The feedback loop model in Figure 1 consists of a forward gain function, $(\hat{q}_o/\hat{q}_r)_f$, and a backward gain function, $(\hat{q}_r/\hat{q}_o)_b$.

The backward gain function is the complex ratio of the output acoustic volume velocity and the input aerodynamic volume velocity and it represents the acoustic response function of the cavity. The backward gain function can be formulated according to the type of resonator involved in the system. The type of cavity resonator considered in the present study is a Helmholtz resonator. A sketch of the cavity is shown in Figure 2. The Helmholtz resonator is composed of a void cavity with an open neck. It is the acoustical analog of a single-degree-of-freedom oscillator. The equivalent damping ratio is governed by both the radiation resistance of the orifice and viscous losses in the orifice. The resonance frequency, which is equal to the natural frequency, depends on the equivalent mass of the fluid within the neck and on the equivalent compliance of the compressed fluid within the cavity. The equivalent mass also accounts for the radiation reactance, and flow entrainment in the vicinity of the neck. The compliance depends primarily on cavity volume [18]. Mast and

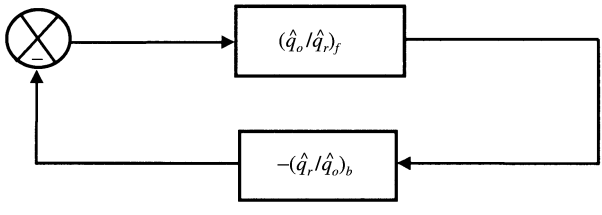


Figure 1. Non-linear feedback loop model of the flow-excited cavity.

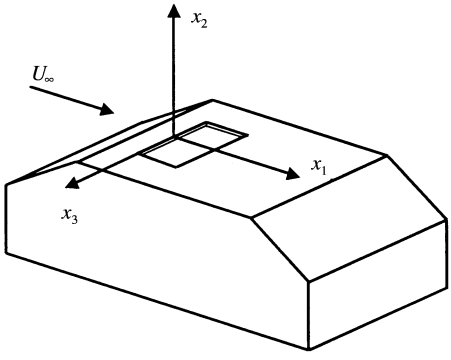


Figure 2. Co-ordinates system and cavity geometry.

Pierce derived a backward gain function in terms of the angular resonance frequency of the Helmholtz resonator, $\omega_r$, and the damping ratio, $\zeta$, of the equivalent single-degree-of-freedom system. The backward gain function can be represented as [15]

$$\left(\frac{\hat{q}_r}{\hat{q}_o}\right)_b = \frac{-(2\zeta(\mathrm{j}\omega)\omega_r + \omega_r^2)}{(\mathrm{j}\omega)^2 + 2\zeta(\mathrm{j}\omega)\omega_r + \omega_r^2}. \tag{2}$$

In the present study, the above backward gain function was used in the feedback loop analysis together with a forward gain function that will be derived in the next section.

## 3. FORMULATION OF THE FORWARD GAIN FUNCTION

The forward gain function is the complex ratio of the output aerodynamic volume velocity and the input acoustic volume velocity. It represents the external pressure fluctuations of the flow instability triggered by the acoustic flow (i.e., if the output volume velocity is replaced by the output pressure). In the present study, vortex sound theory [9, 10] was used to model the periodic pressure fluctuations induced by vortices convected over the cavity orifice.

### 3.1. VORTEX SOUND THEORY

Vortex sound theory describes the power transfer mechanism between the vortical flow field and the acoustic flow field. For low Mach number flows, the vortical flow can be assumed to be incompressible. The instantaneous acoustic power, $P$, transferred from the incompressible vortical flow and by the mean flow to the compressible potential acoustic flow is given by

$$P = -\rho \int_v (\boldsymbol{\omega} \times \mathbf{v}) \cdot \mathbf{u} \, \mathrm{d}\upsilon, \tag{3}$$

where $\bar{\omega} = \nabla \times \mathbf{v}$ is the vorticity vector, $\mathbf{v}$ is the local flow velocity vector, and $\mathbf{u}$ is the local acoustic velocity vector. The integral is carried out over the volume, $\upsilon$, where the vorticity $\boldsymbol{\omega}$ is non-vanishing. The power is transferred from the vortical flow (and the mean flow) to

the acoustic field through the Magnus force, $-\rho(\boldsymbol{\omega}\times\mathbf{v})$, acting on fluid elements throughout. It should be noted that a positive value of the scalar product of the force, $-\rho(\boldsymbol{\omega}\times\mathbf{v})$, and the acoustic velocity vector, $\mathbf{u}$, indicates a net work production.

### 3.2. PERIODIC EXTERNAL EXCITATION PRESSURE

To make use of the interpretation of vortex sound theory in the present formulation, the flow over the cavity is simplified as a train of discrete line vortices travelling at a constant convection speed $U_c$: the local flow velocity at the center of a vortex can be represented as

$$\mathbf{v} = U_c\mathbf{n}_1, \tag{4}$$

where $\mathbf{n}_i$, $i = 1, 2, 3$ represents the unit vector in the $x_i$ direction of the co-ordinate system shown in Figure 2. Since the flow can be assumed to be nearly two-dimensional over the orifice, only the vorticity component in the spanwise direction (i.e., in the $x_3$ direction) needs to be considered. Thus, the vorticity vector is

$$\boldsymbol{\omega} = \Omega\mathbf{n}_3. \tag{5}$$

The transverse force per unit span induced by the vortices on the compressible flow in the cavity can thus be calculated as follows:

$$\mathbf{F}_{ext} = \int_S -\rho(\boldsymbol{\omega}\times\mathbf{v})\,\mathrm{d}S = \int_S -\rho(\Omega\mathbf{n}_3\times U_c\mathbf{n}_1)\,\mathrm{d}S = \left(-\rho U_c\int_S \Omega\,\mathrm{d}S\right)\mathbf{n}_2 = (-\rho\Gamma U_c)\mathbf{n}_2, \tag{6}$$

where $\Gamma = \int_S \boldsymbol{\omega}\cdot\mathbf{n}_3\,\mathrm{d}S$ is the vortex circulation, and $S$ is the cross-sectional area (along the $x_1$–$x_2$ plane) of a control volume enclosing the orifice. The control volume shown in Figure 3 is the region of interest where interactions between the vortical flow and the acoustic flow are presumed to be strong. The circulation is simply the integral of the vorticity (i.e., $\Gamma = \int_S \Omega\mathbf{n}_3\cdot\mathbf{n}_3\,\mathrm{d}S = \int_S \Omega\,\mathrm{d}S$). It is negative for the co-ordinate system shown in

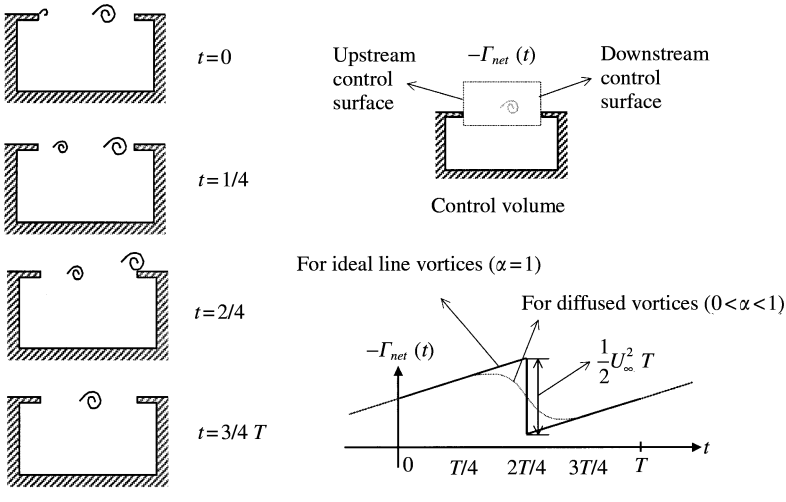


Figure 3. A diagram of circulation strength fluctuations.

Figure 2. Therefore, the vortices convected downstream over the orifice induce a lifting force pointing out of the cavity orifice in the positive $x_2$ direction. The local non-uniform pressure distribution induced by the discrete vortices across the orifice at any instant can be integrated over the orifice to yield an overall pressure fluctuation as a function of time. The excitation pressure, $p_{ext}$, can be obtained by dividing the Magnus force in equation (6) by the streamwise orifice length, $d$:

$$p_{ext}\mathbf{n}_2 = -\frac{\mathbf{F}_{ext}}{d} \tag{7a}$$

and thus,

$$p_{ext} = \frac{\rho \Gamma U_c}{d}. \tag{7b}$$

Positive and negative signs in the external force, $\mathbf{F}_{ext}$, mean upward and downward lift forces, respectively, in the chosen co-ordinate system (see Figure 2). The sign convention has been changed in equation (7a) so that positive and negative pressures represent compression and rarefaction respectively. Note that equation (7b) is in fact Kutta–Joukowski's law. The effect of the external pressure, $p_{ext}$, is analogous to that of an evenly distributed external pressure, such as that produced by a normally incident plane wave.

Recall that equation (7) was formulated based on the assumption of ideal line vortices (i.e., concentrated vortices). However, equation (7) is assumed to be valid in the practical case where vortices are diffused. In either case, the circulation $\Gamma$ represents the total circulation strength within the control volume and the velocity $U_c$ represents the constant convection velocity of the vortices within the control volume. Then, from equation (7b), it can be seen that the external pressure is in phase with and proportional to the total circulation strength within the control volume.

### 3.3. CIRCULATION STRENGTH BALANCE

The net circulation strength within the control volume enclosing the cavity orifice, where the interaction between the acoustic flow and the vortically induced flow is strong, is investigated in this subsection. If the flow within the control volume is assumed to be inviscid (i.e., no generation or dissipation of vorticity within the control volume), then the Reynolds transport theorem applied to the circulation within the control volume yields

$$\frac{\mathrm{d}}{\mathrm{d}t}\iint_{c.v.} \Omega \,\mathrm{d}S = \left(\int_{c.v.} \Omega v_1 \,\mathrm{d}x_2\right)_{in} - \left(\int_{c.v.} \Omega v_1 \,\mathrm{d}x_2\right)_{out}. \tag{8a}$$

The above equation shows that the net rate of change of circulation within the control volume is the sum of the influx of circulation and the outflux of circulation. The influx is originally distributed throughout the incoming boundary layer and shed into the cavity orifice area through the upstream control surface. The outflux is carried primarily by the discrete vortices which are discharged from the control volume crossing the downstream control surface.

Equation (8a) can be rewritten in terms of the circulation, $\Gamma_{net}(t) = \iint_{c.v.} \Omega \,\mathrm{d}S$, recognizing that the flux terms become $\dot{\Gamma}_{in}(t) = (\int_{c.s.} \Omega v_1 \,\mathrm{d}x_2)_{in}$ and $\dot{\Gamma}_{out}(t) = (\int_{c.v.} \Omega v_1 \,\mathrm{d}x_2)_{out}$, i.e.,

$$\dot{\Gamma}_{net}(t) = \dot{\Gamma}_{in}(t) - \dot{\Gamma}_{out}(t). \tag{8b}$$

The circulation influx at the upstream edge, $\dot{\Gamma}_{in}(t)$, can be approximated as a function of the free stream flow velocity, $U_\infty$, as explained by Nelson and his colleagues [17], i.e.,

$$\dot{\Gamma}_{in}(t) = \int_0^{\delta_b} \Omega v_1 \, \mathrm{d}x_2 = \int_0^{\delta_b} \left( \frac{\partial v_2}{\partial x_1} - \frac{\partial v_1}{\partial x_2} \right) v_1 \, \mathrm{d}x_2 = \int_0^{\delta_b} -\frac{\mathrm{d}v_1}{\mathrm{d}x_2} v_1 \, \mathrm{d}x_2 = \int_0^{\delta_b} -v_1 \, \mathrm{d}v_1 = -\frac{1}{2} U_\infty^2, \tag{9}$$

where $\delta_b$ represents the boundary layer thickness and $v_i$ represents the flow velocity component in the $x_i$ direction. Note that the circulation influx is independent of the velocity profile $v_1(x_2)$ and is a constant for a given free stream flow velocity as can be seen in equation (9). Therefore, it is the unsteady circulation outflux at the downstream control surface that is responsible for the fluctuations of the net circulation within the control volume.

The time history of the net circulation fluctuations, along with a series of schematic diagrams for the convection of vortices over one cycle are given in Figure 3. Vortex shedding is triggered by periodic acoustic velocity near the upstream edge. It has been frequently reported that it occurs at the moment the acoustic component of the flow, the real part of $\hat{q}_r \, \mathrm{e}^{\mathrm{j}\omega t}$, is zero and increasing [2, 15, 17]. The time origin ($t = 0$) was chosen as the moment when a vortex is shed near the upstream edge. The input acoustic velocity is considered nearly sinusoidal since a cavity resonator can be considered a low-pass filter. The time history of the net circulation is represented by a solid line in the case of convection of ideal line vortices. Whenever a vortex is discharged at the downstream control surface, the net circulation experiences a rapid increase in amplitude (which occurs at $t = 2/4T$ in Figure 3). The vorticity is accumulated at a constant rate over the rest of the cycle. Note that the circulation outflux (and thus the net circulation) can be considered as a periodic function since the vortical flow over the cavity orifice is synchronized with the action of the acoustic flow: that is,

$$\dot{\Gamma}_{out}(t) = \dot{\Gamma}_{out}(t - nT), \tag{10}$$

where $n$ is an integer, and $T$ is the acoustic period.

### 3.4. FOURIER SERIES REPRESENTATION

Since the circulation outflux is a periodic function, it can be represented as a Fourier series, i.e.,

$$\dot{\Gamma}_{out}(t) = \sum_{n=-\infty}^{\infty} C_n \, \mathrm{e}^{\mathrm{j}(2\pi n/T)t} \tag{11}$$

with the Fourier coefficients,

$$C_n = \frac{1}{T} \int_T \dot{\Gamma}_{out}(t) \, \mathrm{e}^{-\mathrm{j}(2\pi n/T)t} \, \mathrm{d}t. \tag{12}$$

The rate of net circulation can be represented by substituting equations (9) and (11) into equation (8b), i.e.,

$$\dot{\Gamma}_{net}(t) = -\sum_{\substack{n=-\infty \\ n \neq 0}}^{\infty} C_n \, \mathrm{e}^{-\mathrm{j}(2\pi n/T)t}. \tag{13}$$

Note that the DC term of the Fourier series of the rate of net circulation was nullified since there can be no net accumulation of circulation within the control volume during one complete acoustic cycle (that is, $C_0 = \dot{\Gamma}_{in}(t) = -\frac{1}{2}U_\infty^2$). Then, the net circulation can be obtained by integrating equation (13) with respect to time, i.e.,

$$\Gamma_{net}(t) = \overline{\Gamma_{net}} - \sum_{\substack{n=-\infty \\ n\neq 0}}^{\infty} \left(\frac{T}{\mathrm{j}2\pi n}\right) C_n \, \mathrm{e}^{\mathrm{j}(2\pi n/T)t}, \tag{14}$$

where $\overline{\Gamma_{net}}$ is an integrating constant and represents the time-averaged net circulation. The mean value of the net circulation within the control volume can be obtained by multiplying the steady circulation influx and the time during which a vortex is convected over the orifice, i.e.,

$$\overline{\Gamma_{net}} = -\frac{1}{2} U_\infty^2 \frac{d}{U_c}. \tag{15}$$

Finally, the external excitation pressure, $p_{ext}$, can be obtained by combining equations (7b) and (14), i.e.,

$$p_{ext}(t) = -\frac{1}{2}\rho U_\infty^2 - \rho \frac{U_c}{d} \sum_{\substack{n=-\infty \\ n\neq 0}}^{\infty} \left(\frac{T}{\mathrm{j}2\pi n}\right) C_n \, \mathrm{e}^{\mathrm{j}(2\pi n/T)t}. \tag{16}$$

The time history of the net circulation as well as that of the external excitation pressure depend on both the details of the distribution of the vorticity within the discrete vortices and the vortices' convection speed. For instance, when a loosely packed vortex is discharged out of the control volume, the net circulation within the control volume would not change rapidly compared to the case when a tightly packed vortex is discharged (see in Figure 3 the time history of the net circulation for the case of diffused vortices represented by a dotted line). In the next subsection, two circulation outflux functions associated with the convection of ideal vortices and diffused vortices, respectively, are investigated. In either case, the vortices' convection velocity is assumed to be constant.

### 3.5. MODELLING OF THE EFFECTS OF VORTEX DIFFUSION

The simple case of ideal line vortices was first considered. If the vorticity shed during one period of an acoustic cycle is perfectly concentrated along a line, following an ideal rolling-up process, the circulation outflux can be expressed as

$$\dot{\Gamma}_{out}(t) = -\tfrac{1}{2}U_\infty^2 T\delta(t-\tau), \qquad \dot{\Gamma}_{out}(t-nT) = \dot{\Gamma}_{out}(t), \tag{17}$$

where $\delta(t)$ is the Dirac delta function and $\tau$ is the convection time delay given by $\tau = d/U_c$ (alternatively, $\tau = (\mathrm{St}_\phi/2\pi)T$ where $St_\phi$ is a Strouhal number given by $St_\phi = \omega d/U_c$). The resulting external pressure fluctuation associated with the convection of ideal line vortices can be expressed as

$$p_{ext}(t) = -\frac{1}{2}\rho U_\infty^2 + \frac{1}{2}\rho U_\infty^2 \sum_{\substack{n=-\infty \\ n\neq 0}}^{\infty} \frac{1}{\mathrm{j}nSt_\phi} \mathrm{e}^{\mathrm{j}n(\omega t - \mathrm{St}_\phi)}. \tag{18}$$

Since, in general, the external pressure, $p_{ext}(t)$, is a non-sinusoidal periodic function as can be seen in equation (18), the aerodynamic volume velocity associated with the external pressure is also a non-sinusoidal periodic function because they are linearly related. Since the output aerodynamic volume velocity resulting from the nearly sinusoidal acoustic volume velocity input consists in not only the fundamental component but also its harmonic components plus a DC term, the subsystem modelled by the forward gain function is considered non-linear. In the describing function analysis of non-linear systems, the output is approximated by the fundamental component and the higher order harmonic terms are discarded [19]. The phasor of the fundamental component of the external excitation pressure can be written as

$$\hat{p}_{ext} = \rho U_\infty^2 \frac{1}{\mathrm{St}_\phi} \mathrm{e}^{-\mathrm{jSt}_\phi}. \tag{19}$$

Exact modelling of the circulation outflux function for the practical case of diffused vortices may require a detailed knowledge of the interaction between the vortical flow and the resulting acoustic flow *a priori*. However, considering the simplicity of the control volume model used in the present work, the approach of obtaining the circulation outflux based on both the details of the vorticity distribution in a diffused vortex and its convection is considered unnecessary. Instead, a simple form of the circulation outflux function is given to stimulate the case when a diffused vortex is discharged out of the control volume. The circulation outflux function tested in the present work to simulate the case of a diffused vortex is a rectangular step function and is given by

$$\begin{aligned} \dot{\Gamma}_{out}(t) &= -H \quad (-W/2 + \tau \leqslant t \leqslant W/2 + \tau), \\ \dot{\Gamma}_{out}(t) &= 0 \quad \text{(otherwise)}, \\ \dot{\Gamma}_{out}(t - nT) &= \dot{\Gamma}_{out}(t), \end{aligned} \tag{20}$$

where $H$ is given by $H = \frac{1}{2} U_\infty^2 T/W$, and $W$ is a control parameter that is greater than zero and less than or equal to $T$. The control parameter, $W$, controls the degree to which the vortex is concentrated: that is, the vortex becomes an ideal line vortex as $W$ goes to zero while the circulation outflux becomes uniform when $W$ is given by $W = T$. The external pressure fluctuation resulting from the above assumed circulation outflux can be obtained from a Fourier transform of equation (20), and substitution of the Fourier coefficients into equation (16), i.e.,

$$p_{ext}(t) = -\frac{1}{2}\rho U_\infty^2 + \frac{1}{2}\rho U_\infty^2 \sum_{\substack{n=-\infty \\ n \neq 0}}^{\infty} \frac{1}{\mathrm{j}n\mathrm{St}_\phi} sinc\left(\frac{nW}{T}\right) \mathrm{e}^{\mathrm{j}n(\omega t - \mathrm{St}_\phi)}, \tag{21}$$

where $sinc(x)$ is defined as $sinc(x) = \sin(\pi x)/\pi x$. The phasor of the fundamental component of the fluctuating terms can be identified in equation (21) as

$$\hat{p}_{ext} = \rho U_\infty^2 \frac{1}{\mathrm{St}_\phi} sinc\left(\frac{W}{T}\right) \mathrm{e}^{-\mathrm{jSt}_\phi}. \tag{22}$$

Note that, when $W = 0$ (i.e., in the case of an ideal line vortex), equation (22) becomes identical to equation (19) as expected. As $W$ increases (i.e., as the vortex becomes more diffuse), the amplitude of the phasor decreases and finally reaches zero as $W$ approaches the value of $T$ (i.e., the circulation outflux becomes steady as the vortices are fully diffused).

Thus the effect of vortex diffusion is to decrease the amplitude of the external pressure fluctuation as can be seen in equation (22). A similar result is obtained as long as the assumed circulation outflux is given by a function symmetric with respect to $t = \tau$. A symmetric circulation outflux function may represent, for instance, a symmetrically distributed vorticity field convected at a constant speed. In the case of an asymmetric circulation outflux function, the phase of the fundamental component of the external pressure fluctuation would vary from that specified in equation (22). That would in turn result in a change in the oscillation frequency. The circulation outflux function is assumed to be symmetric in the present work. This assumption is consistent with experimental results reported in a previous study [20] showing that the pulsation amplitude of a flow-excited cavity tends to decrease without significant changes in the oscillation frequency as the shear layer thickness (i.e., diffusivity of a vortex) increases. Then, the phasor of the fundamental component of the external pressure fluctuation can be rewritten for general cases of symmetrical circulation outflux functions by introducing a parameter $\alpha$, i.e.,

$$\hat{p}_{ext} = \alpha \rho U_\infty^2 \frac{1}{\mathrm{St}_\phi} \mathrm{e}^{-\mathrm{jSt}_\phi}. \tag{23}$$

The parameter $\alpha$ represents the degree to which a vortex is concentrated. It reaches a maximum value of unity for an ideal line vortex, and is minimum or null for a totally diffused vortex.

### 3.6. DESCRIBING FUNCTION THEORY

The phasor of the fundamental component of the external pressure fluctuation, $\hat{p}_{ext}$, can be related to the phasor of the fundamental component of the aerodynamic excitation volume velocity, $\hat{q}_o$, through the relation [15]

$$\hat{q}_o = S_o^2 \hat{p}_{ext}/(\mathrm{j}\omega M), \tag{24}$$

where $M$ is the effective mass of the Helmholtz resonator. This is simply the linearized momentum equation for sinusoidal flow through the orifice in the absence of a cavity, neglecting the effects of sound radiation and the orifice resistance (i.e., assuming the orifice to have a purely mass-like impedance). Equation (24) can be rewritten by using equation (23), i.e.,

$$\hat{q}_0 = \frac{S_o^2 \alpha \rho U_\infty^2}{\mathrm{St}_\phi(\mathrm{j}\omega M)} \mathrm{e}^{-\mathrm{jSt}_\phi}. \tag{25}$$

The phasor of the sinusoidal input is readily obtained recalling that the time origin ($t = 0$) is the moment when the acoustic component of the flow is zero and increasing at this instant, i.e.,

$$\hat{q}_r = |\hat{q}_r|. \tag{26}$$

The forward gain function can be obtained by combining equations (25) and (26), i.e.,

$$\left(\frac{\hat{q}_o}{\hat{q}_r}\right)_f = \frac{S_o^2 \alpha \rho U_\infty^2 1}{\mathrm{St}_\phi(\mathrm{j}\omega M)|\hat{q}_r|} \mathrm{e}^{-\mathrm{jSt}_\phi}. \tag{27a}$$

Interestingly, the forward gain function expressed in equation (27a) is almost identical with that proposed by Mast and Pierce [15], i.e.,

$$\left(\frac{\hat{q}_o}{\hat{q}_r}\right)_f = \frac{S_o^2 \beta \rho U_\infty^2}{\omega M |\hat{q}_r|} e^{-j(3\pi/2 - St_\phi)}. \tag{27b}$$

In combination with the backward gain function expressed in equation (2), equations (27a, b) would predict the same oscillation frequencies and nearly identical oscillation amplitudes over a range of free stream flow velocities provided that the parameter $\beta$ (whose physical interpretation is similar to $\alpha$ in the present work) is set equal to $\alpha/St_\phi$ for a given free stream velocity. Mast and Pierce's derivation of equation (27b) was based on the concept of "vortex-edge interaction" mechanism: that is, the dipole-like aerodynamic pressure oscillation near the downstream edge on which the vortices periodically impinge was considered responsible for the acoustic excitation of the cavity. In their work, the phase response of the forward gain function was modelled as the linear combination of a convection phase lag and an inherently constant phase factor associated with the vortex-edge interaction mechanism. In equation (27b), the exponent $St_\phi$ represents the phase lag associated with the convection time for a vortex to travel from the upstream edge to the downstream edge of the cavity orifice, while $e^{j3\pi/2}$ is the inherent phase factor between $\hat{q}_o$ and $\hat{q}_r$ when a vortex interacts with the downstream edge. To obtain the phase factor associated with the vortex-edge interaction, Mast and Pierce referred to the experimental results presented by Tang and Rockwell [21], who studied the instantaneous pressure fields along the top and front faces of a corner as a function of the streamwise position of an approaching vortex.

When they interpreted the flow visualization results obtained by Tang and Rockwell, they judged a vortex to "reach" the downstream edge at the instant when the leading edge of the vortex, not the core of the vortex, reaches the edge. However, the consistency of this vortex impingement criterion with the rest of their discussion is disputable, since it was assumed in their study that the vortices travel a distance, $d$, to obtain the convection phase lag. When the pressure gradient along the corner at the moment where the vortex core reached the downstream edge in Tang and Rockwell's visualization study is used, it can be found that Mast and Pierce's approach would yield a far different phase factor of $e^{j\pi/2}$.

In the present work, the forward gain function was derived based on a different physical basis; a circulation strength balance over the cavity orifice. This approach appears to be preferable over that of reference [15]. The phase response of the forward gain function does not need to be modelled separately from the amplitude gain, and the phase factor, $e^{j3\pi/2}$, has a clearer physical interpretation (i.e., a mass-like impedance of the air within the orifice of a cavity).

## 4. SOLUTION PROCEDURE AND STABILITY ANALYSIS

### 4.1. GRAPHICAL SOLUTION OF LIMIT CYCLES

The oscillation frequencies and the amplitudes of the so-called "limit cycles" (i.e., nearly sinusoidal oscillation in a non-linear system) of the flow-excited resonator system can be obtained by solving the characteristic equation of the feedback loop shown in Figure 1, i.e.,

$$\left(\frac{\hat{q}_r}{\hat{q}_o}\right)_b \left(\frac{\hat{q}_o}{\hat{q}_r}\right)_f = 1. \tag{28}$$

This equation represents the self-consistent condition of any closed feedback loop. For the purpose of calculating the oscillation frequency and the amplitude, the non-linear describing function, $(\hat{q}_o/\hat{q}_r)_f$, equation (27), was decomposed into linear and non-linear elements. The linear element of the forward gain function was then combined with the linear backward gain function to yield a new linear gain function, $G(j\omega)$, expressed as

$$G(j\omega) = K_p \frac{\omega_r^2 + 2\zeta\omega_r(j\omega)}{j\omega((j\omega)^2 + 2\zeta\omega_r(j\omega) + \omega_r^2)} e^{-(j\omega)\tau}, \tag{29}$$

where $K_p$ is a constant gain defined as $K_p = \alpha\rho U_\infty^2 S_o^2/\tau M$. Note that the linear gain function in equation (29) also includes an integrator and a time delay. Then, the non-linear element in the forward gain function can be represented as

$$N(A, \omega) = \frac{1}{\omega A}, \tag{30}$$

where $A$ represents the amplitude of the input sinusoidal signal (i.e., $A = |\hat{q}_r|$). By using equations (29) and (30), equation (28) can be conveniently rearranged as

$$1 + N(A, \omega)\, G(j\omega) = 0 \tag{31a}$$

or equivalently,

$$G(j\omega) = -\frac{1}{N(A, \omega)}. \tag{31b}$$

Then, the characteristic equation, equation (31b), can be solved graphically by using Nyquist plots. From polar plots of the open-loop responses of the two gain functions, $G(j\omega)$ and $-1/N(A, \omega)$, the values of frequency and amplitude that satisfy equation (31) can be uniquely determined at each crossing point of the two curves.

Typical Nyquist plots for $G(j\omega)$, equation (29), are shown in Figure 4 for four different free stream flow velocities. The negative real axis in each polar plot represents the locus of $-1/N(A, \omega)$ (i.e., $-1/N(A, \omega) = -\omega A$ from equation (30)). Note that the shape of the frequency response of the linear gain function, $G(j\omega)$, is a spiral because it includes a time delay element. $G(j\omega)$ crosses the negative real axis repeatedly. Thus, given a free stream flow velocity, there is an infinite number of possible limit cycles, even though the predicted amplitude of the limit cycle goes to zero rapidly as its oscillation frequency increases as can be seen in Figures 4(a)–(d). Each limit cycle is associated with a different shear layer excitation mode. The first shear layer excitation mode has approximately one vortex over the orifice and is associated with the second limit cycle (when the limit cycles are numbered in the order of increasing oscillation frequency). The second shear layer excitation mode has approximately two vortices over the orifice and is associated with the third limit cycle, and so on. The shear layer excitation mode that is associated with the first limit cycle with the lowest oscillation frequency among the limit cycles is referred to as the shear layer excitation mode "zero" in the present work. Its wavelength is theoretically greater than four times the orifice length, $d$, in the streamwise direction [22]. In the next subsection, the stability of the limit cycles is assessed by using the Nyquist stability criterion.

### 4.2. NYQUIST STABILITY CRITERION

Very few researchers have theoretically investigated the stability of the flow-excited oscillation. The stability of a limit cycling system is of particular interest here since it allows

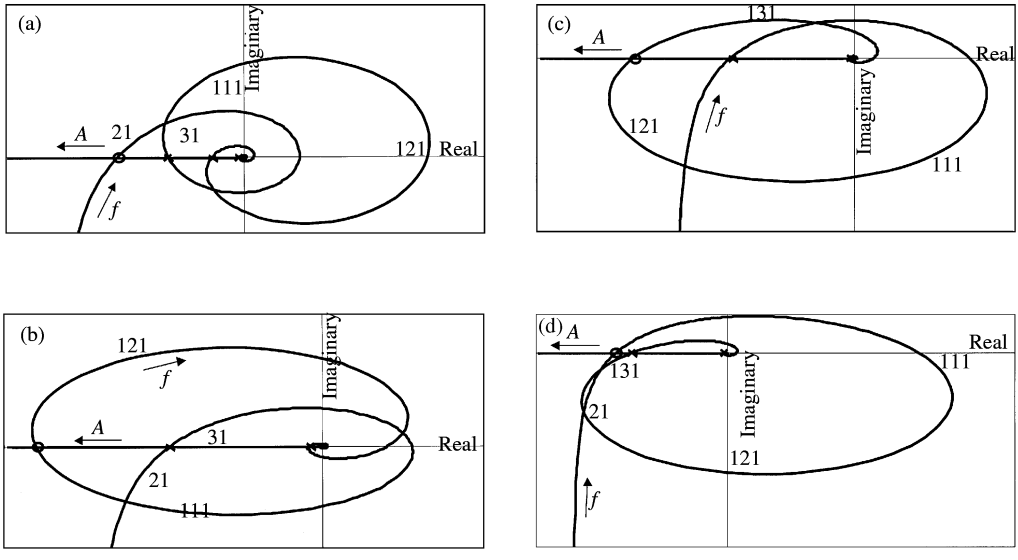


Figure 4. Nyquist plots (polar plots) of the function $G(j\omega)$ given by equation (29) in the case where $d = 8$ cm (thus $\omega_r = 754$ and $\zeta = 0{\cdot}0455$: see Table 1); (a) $U_\infty = 15$ m/s; (b) $U_\infty = 20$ m/s; (c) $U_\infty = 25$ m/s; (d) $U_\infty = 30$ m/s.

the prediction of the onset and termination velocities for different modes of flow excitation. Covert [23] and Howe [6] attempted to predict the onset velocity of different shear layer modes by using linear stability theory. However, Covert's model cannot predict the termination velocity. Moreover, both of their models cannot predict the existence of a stable second shear layer excitation mode coupled with the fundamental acoustic mode, which was observed over a range of low free stream flow velocities in the experiment performed in the present work (detailed experimental results will be discussed in section 5). In the present work, attempts were made to predict the onset and termination velocities for each shear layer excitation mode by using a stability analysis based on the Nyquist stability criterion that can be performed within the framework of the feedback loop model represented in Figure 1. Readers who are not familiar with the Nyquist stability criterion can refer to reference [24], for example.

In order to analyze the stability of the possible limit cycles based on the Nyquist stability criterion, the complete polar plot of the frequency response function, $G(j\omega)$, should be obtained for the whole range of $\omega$ including the region where $0^- < \omega < 0^+$. The complete polar plot of $G(j\omega)$ can be obtained by mapping a so-called Nyquist path defined in the $s$ plane into the $G(s)$ plane. Since the open-loop transfer function, $N(A, \omega)G(s)$ has a pole at the origin in the $s$-plane, the Nyquist path should be chosen such that it circles around the $s = 0$ point, while ensuring that all the poles and zeros of $G(s)$ in the right-half plane are enclosed by the path. A Nyquist path that satisfies these requirements is shown in Figure 5: the Nyquist path describes an infinitesimally small semi-circle near the origin in the $s$ plane to avoid the singularity at the origin. The small semi-circle of the Nyquist path shown in Figure 5 can be represented as $s = \varepsilon e^{j\theta}$ $(-\pi/2 \leqslant \theta \leqslant \pi/2)$, where $\varepsilon$ is its radius. Then, by using equation (29), the map of the semi-circle in the $G(s)$ plane can be represented as

$$G(\varepsilon e^{j\theta}) = K_p \frac{\omega_r^2 + 2\zeta\omega_r\varepsilon e^{j\theta}}{\varepsilon e^{j\theta}(\varepsilon^2 e^{2j\theta} + 2\zeta\omega_r\varepsilon^{j\theta} + \omega_r^2)} e^{-\varepsilon e^{j\theta}\tau}. \tag{32}$$

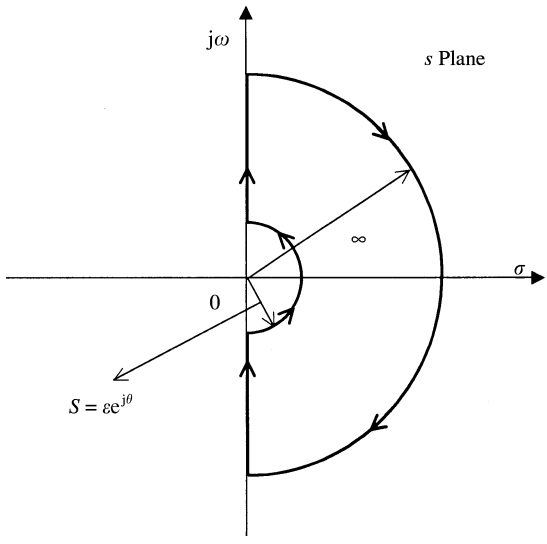


Figure 5. Modified Nyquist path in the $s$ plane.

As $\varepsilon$ tends to zero, equation (32) becomes

$$G(\varepsilon e^{j\theta}) = K_p \frac{\omega_r^2}{\varepsilon e^{j\theta} \omega_r^2} = K_p r e^{-j\theta}, \tag{33}$$

where $r$ tends to infinity as $\varepsilon$ approaches zero. Therefore, the small counterclockwise semi-circle in the right-half $s$ plane is mapped into a large clockwise semi-circle in $G(s)$ plane. The incomplete polar plot of $G(j\omega)$ that is shown in Figure 4(a), for instance, can then be completed by using the above result and the complete polar plot is shown in Figure 6.

Note that equation (31a) represents the characteristic equation of the system, and that only $G(j\omega)$ depends on the variable $j\omega$. Provided that non-linearities involved in the system are independent of the complex variable $j\omega$, $N(A, \omega)$ can be considered a constant gain in the loop transfer function. The same arguments as used in the ordinary Nyquist stability criterion can be applied to the non-linear system except that the number of clockwise encirclements of $G(j\omega)$ around the cross points with $-1/N(A, \omega)$, instead of $(-1, j0)$, should now be counted. An extended Nyquist stability criterion can be interpreted in this case as follows [24]. If points near a limit cycle point and along the increasing-$A$ side of the locus of $-1/N(A, \omega)$ are not enclosed by the locus of $G(j\omega)$, then the corresponding limit cycle is deemed stable: otherwise, the limit cycle is deemed unstable. Among the limit cycles shown in Figures 4(a)–(d), only the leftmost limit cycle points on the negative real axis are predicted to yield a stable oscillation according to this criterion. The stable limit cycles are depicted by circles in Figures (a)–(d), while the unstable limit cycles are marked by crosses. Interestingly, the stable limit cycle (thus the corresponding stable shear layer excitation mode) can be seen to migrate as the free stream velocity increases as shown in Figures 4(a)–(d). That is, the first limit cycle is stable as shown in Figure 4(a). As the free stream velocity increases, the first limit cycle point is enclosed by the locus of $G(j\omega)$ and becomes unstable while the second limit cycle point migrates into the stable region of the Nyquist plots as shown in Figures 4(b) and 4(c). The

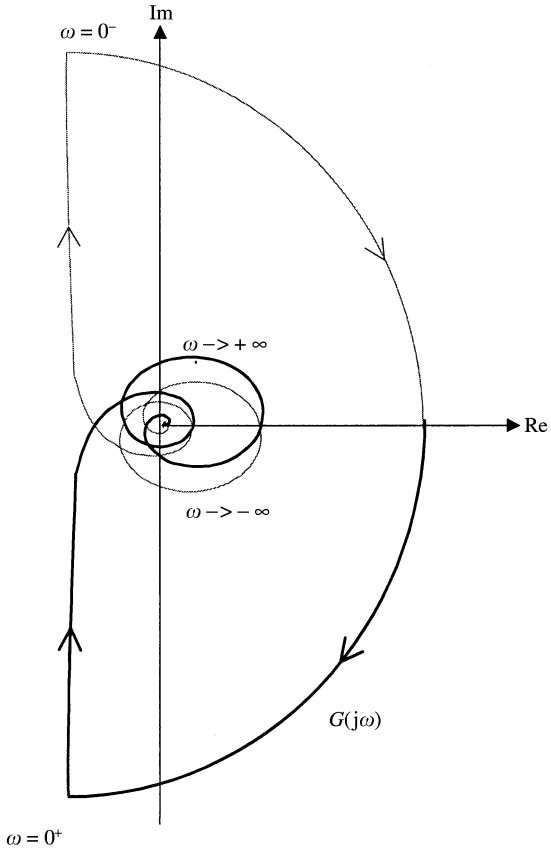


Figure 6. The complete polar plot of the linear gain function $G(j\omega)$ plotted in Figure 4(a).

first limit cycle point migrates back into the stable region at higher velocities as shown in Figure 4(d).

Therefore, only one limit cycle associated with one mode of shear layer excitation is predicted to be stable by the Nyquist stability criterion for each free stream flow velocity. The amplitude of the external pressure fluctuations is predicted to be proportional to $U_\infty^2/\mathrm{St}_\phi$, as shown in equation (27). This results in a $U_\infty^2$ dependence of the excitation pressure amplitude for a given shear layer excitation mode (for instance, $U_\infty^2/\mathrm{St}_\phi \approx U_\infty^2/2\pi$, for the first shear layer excitation mode), which is consistent with the empirical scaling law used by many other researchers. For higher shear layer excitation modes, the excitation pressure is predicted to be still proportional to $U_\infty^2$, but with a different proportionality constant (for instance, $U_\infty^2/\mathrm{St}_\phi \approx U_\infty^2/4\pi$, for the second shear layer excitation mode, and so on). This result can be physically interpreted by the fact that the relative change in total net circulation strength that would result from the discharge of a vortex at the downstream control surface is greater when there is a smaller number of vortices over the orifice. Higher shear layer excitation modes have a large number of vortices over the cavity orifice, and thus produce weaker external pressure fluctuations. This may partly explain why excitation modes higher than the third shear layer mode were not observed in the experimental results reported below.

## 5. RESULTS AND DISCUSSION

Experiments were performed in a low-speed, quiet wind tunnel, using an open cavity, shown in Figure 7, made of 1·1 cm thick Plexiglas. The bases of the two inclined panels were mounted flush with the wind tunnel test section floor. The orifice was rectangular at zero yaw. The orifice size was varied by gluing 1·3 cm thick Plexiglas inserts along the downstream edge of the orifice. The wind tunnel is an Eiffel type with a closed test section and extensive sound attenuation treatment [25]. The test section measured $61 \times 46 \times 152\ \text{cm}^3$. The maximum flow velocity achieved was 50·9 m/s (183·2 km/h) with 1% span-wise uniformity. The average turbulence intensity was 0·1% in the frequency range from 1 Hz to 3 kHz. The overall sound pressure levels in the center of the closed test section, in the absence of the cavity, were 87 dB (79 dBA) and 98 dB (95 dBA) at 26·8 m/s (96·5 km/h) and 50·9 m/s (183·2 km/h) respectively. The background noise was emitted primarily from the wind tunnel fan, at well below the cavity pressure levels of interest. The sound pressure inside the cavity was measured using a Brüel & Kjaer (B&K) type 4133 microphone located 35·6 cm downstream from the front wall in the center of the cavity floor. A B&K type 2609 measuring amplifier was used, the output from which was processed using a Tektronix 2630 frequency analyzer.

The acoustic parameters that are required in the backward gain function expressed by equation (2) were obtained experimentally by measuring the frequency response function of the cavity mounted in the test section of the wind tunnel (with the wind tunnel off). For each case of six different cavity orifice lengths (i.e., $d = 8, 7, 6, 5, 4,$ and 3 cm), the cavity was acoustically excited using a loudspeaker with a random input, and the resonance frequency and the quality factor of the Helmholtz resonator were measured from the frequency response function of the cavity pressure signals. The measured angular resonance frequency, $\omega_r$, and the damping ratio, $\zeta$, for each orifice length are shown in Table 1.

The convection velocity of the vortices, needed in the analytical model, was assumed to be one-half the free stream flow velocity [15, 16]. To verify the above assumption, flow visualization was performed to measure the convection velocity of vortices for one orifice

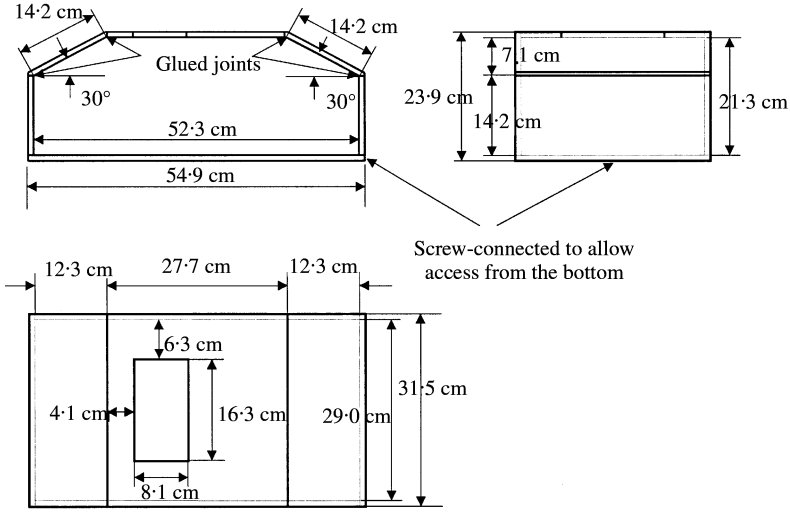


Figure 7. Dimensions of the cavity.

TABLE 1

*Measured angular resonance frequencies and damping ratios of the cavity model in the wind tunnel*

| $d$ (cm) | $\omega_r$ (rad/s) | $\zeta$ |
|---|---|---|
| 8 | 754 | 0·0455 |
| 7 | 722·6 | 0·0625 |
| 6 | 697·4 | 0·05 |
| 5 | 659·7 | 0·0556 |
| 4 | 628·3 | 0·0714 |
| 3 | 603·2 | 0·0714 |

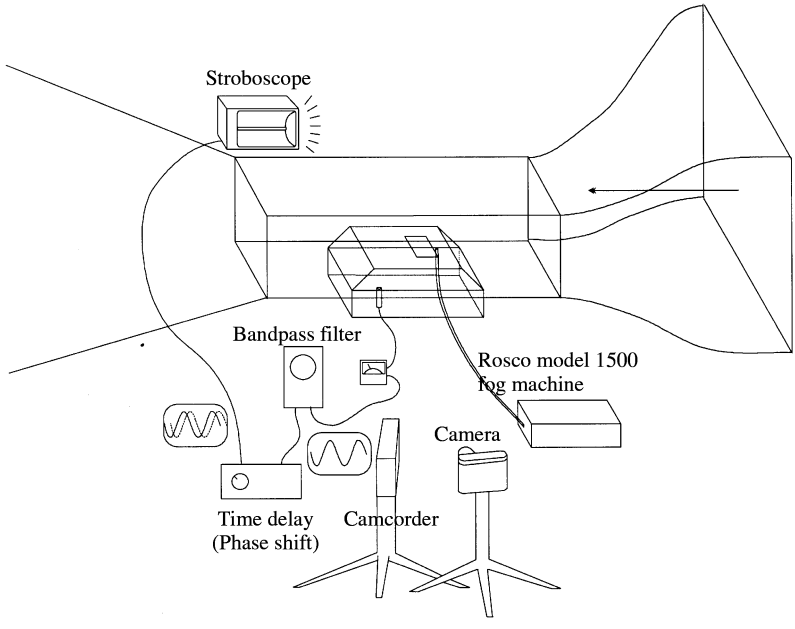


Figure 8. Experimental set-up for flow visualization.

length, $d = 8$ cm (see Figure 8 for the experimental set-up used for the flow visualization). The free stream flow velocity in the test section of the wind tunnel was 20·8 m/s, that was the critical speed at which the amplitude of the acoustic pressure in the cavity was maximum. Using a stroboscope and introducing a time delay between the microphone signals measured inside the cavity and the stroboscope, eight still photos were taken at evenly spaced phase intervals over one cycle of the nearly sinusoidal pressure oscillation in the cavity. A value of $U_c = 0{\cdot}48U_\infty$ was obtained, which was close to the assumed convection velocity.

The sensitivities of the predictions, both in the frequency and in the amplitude of the pressure oscillations inside the cavity, to the ratio of the convection velocity to the free stream flow velocity were investigated and shown in Figures 9(a) and 9(b), respectively, for the case of the opening length $d = 7$ cm. The results of the simulation show that a $\pm$ 10% variation of the convection velocity (i.e., $U_c = 0{\cdot}55U_\infty$ and $U_c = 0{\cdot}45U_\infty$) leads to a 3·1% increase and a 3·7% decrease, respectively, in the value of the frequency prediction at the

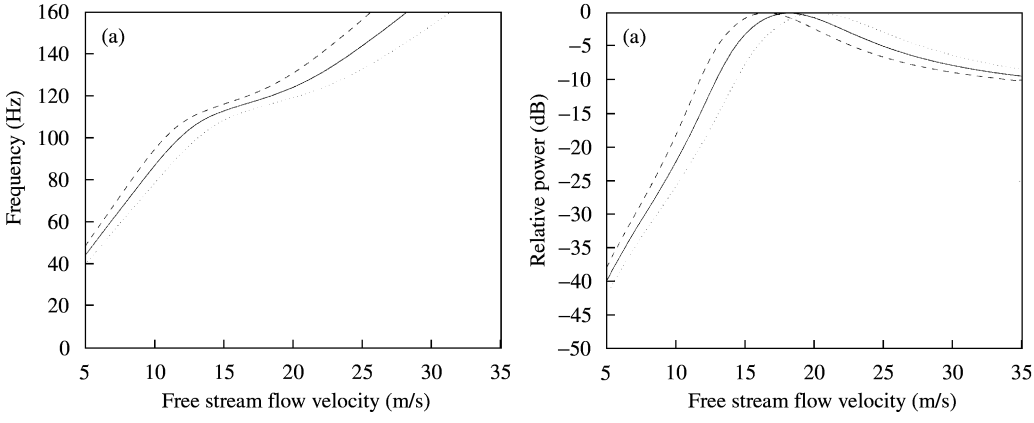


Figure 9. Sensitivities of (a) the frequency prediction and (b) the amplitude prediction to the $\pm$ 10% changes in the ratio of the convection velocity to the mean-flow velocity; $U_c/U_\infty = 0{\cdot}5$ (——); $U_c/U_\infty = 0{\cdot}55$ (– – – –); $U_c/U_\infty = 0{\cdot}45$ (· · · ·). The oscillation frequency and the cavity pressure amplitude were calculated by using equation (28) in combination with equations (2) and (27) in the case where $d = 7$ cm (thus $\omega_r = 722{\cdot}6$ and $\zeta = 0{\cdot}0625$: see Table 1).

critical speed; i.e., 18 m/s for $U_c = 0{\cdot}5U_\infty$ as shown in Figure 9(a). A $\pm$ 10% change of the convection velocity leads to 8·3% decrease and 11% increase, respectively, in the predicted value of the critical velocity as shown in Figure 9(b).

The upper limit of the cavity pressure amplitude can be predicted by setting the vortex concentration parameter $\alpha$ to the maximum value (i.e., $\alpha = 1$ that corresponds to the case of line vortices) in the analytical model. Since an appropriate value of the vortex concentration parameter $\alpha$ cannot be known *a priori*, only the relative amplitudes of the cavity pressure that are normalized with respect to, for instance, the maximum amplitude of the cavity pressure within the range of free stream flow velocities can be predicted. Instead of comparing the normalized data with the normalized predictions, the vortex concentration parameter $\alpha$ was estimated by using absolute cavity pressure amplitudes obtained experimentally over a range of free stream flow velocities for one orifice length. The estimated parameter $\alpha$ was used in all other cases to see how the vortex concentration parameter may change depending on the orifice length. The vortex concentration parameter was estimated as $\alpha = 0{\cdot}25$ for the case where the orifice length $d$ was 7 cm.

For each orifice length, the cavity pressure frequencies and amplitudes were experimentally obtained over a range of free flow velocities (from 5 to 35 m/s). The experimental data along with the theoretical predictions are shown in Figures 10(a)–10(f) and Figures 11(a)–11(f) for the oscillation frequency and the cavity pressure amplitude respectively. For all cases of orifice lengths tested in the present work, the cavity's Helmholtz mode was observed to be excited by the first shear layer excitation mode within the range of free stream flow velocities specified above. For the first three orifice lengths (i.e., $d = 8$, 7, and 6 cm), the cavity's Helmholtz mode was observed to be also excited by the second shear layer excitation mode at low free stream flow velocities. The experimental data plotted in Figures 10 and 11 were obtained from the dominant tonal component in the power spectrum of the cavity pressure, by inspection. Some data points may not represent very "strong" self-excited oscillations due to by their low amplitudes in Figure 11.

The experimental data associated with the first shear layer excitation mode are denoted by circles while data points associated with the second shear layer excitation mode are

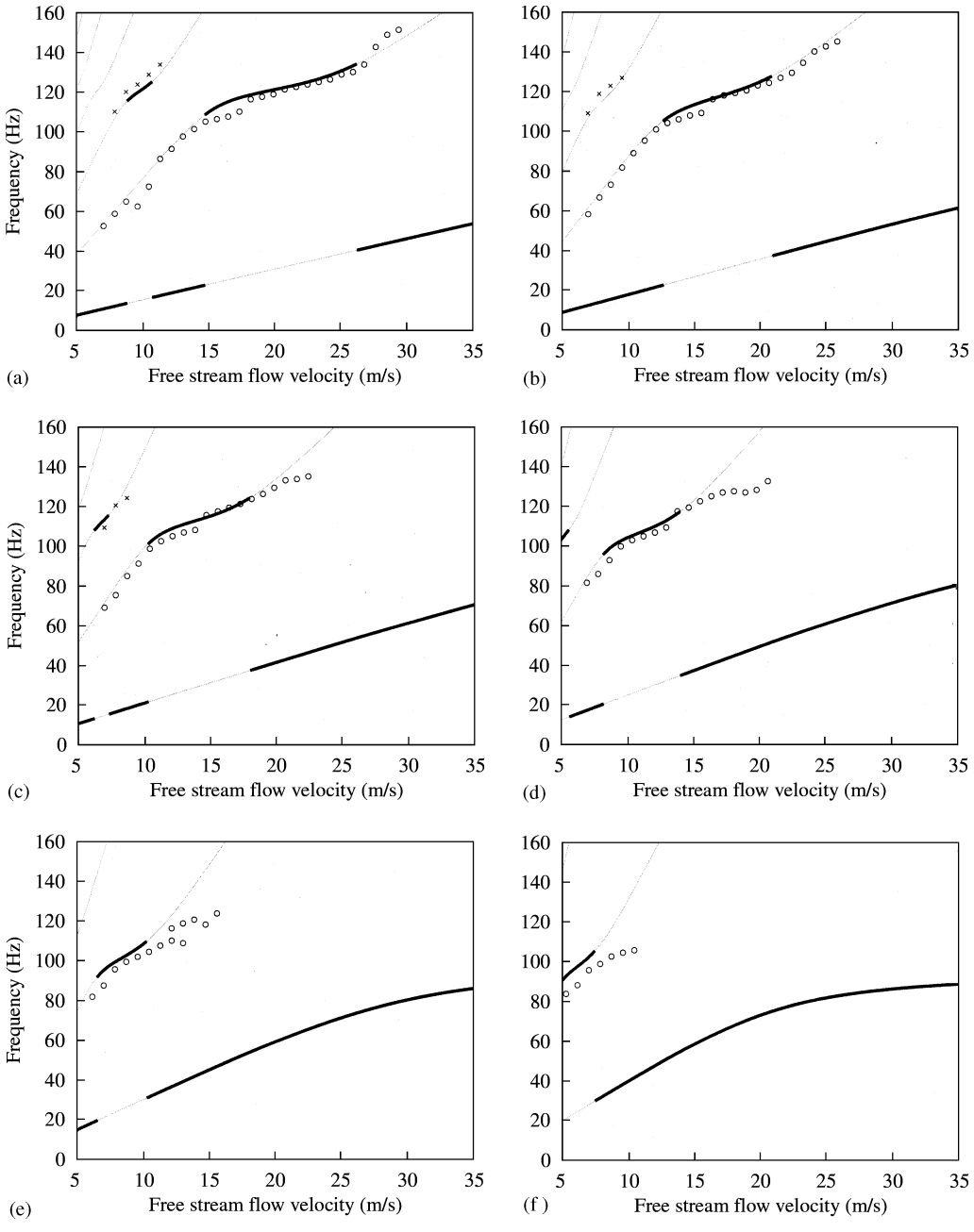


Figure 10. Comparison between the experimental data and the predicted oscillation frequencies for a range of free stream flow velocities in the cases where the orifice length is 8, 7, 6, 5, 4, and 3 cm, respectively, (a)–(f). ○ ○ ○, measured frequencies associated with the first shear layer excitation mode. X's, measured frequencies associated with the second shear layer excitation mode. ——, predicted oscillation frequencies associated with the first and higher shear layer excitation modes. ——, shear layer excitation mode that is predicted to be stable at each free stream flow velocity. (a) $d = 8$ cm; (b) $d = 7$ cm; (c) $d = 6$ cm; (d) $d = 5$ cm; (e) $d = 4$ cm; (f) $d = 3$ cm.

denoted by $x$'s, as shown in Figures 10 and 11. For the amplitude predictions in Figures 11(a) and 11(b), the vortex concentration parameter was assumed to be $\alpha = 0{\cdot}25$. In Figures 10 and 11, the theoretical predictions for the fundamental and higher shear layer excitation

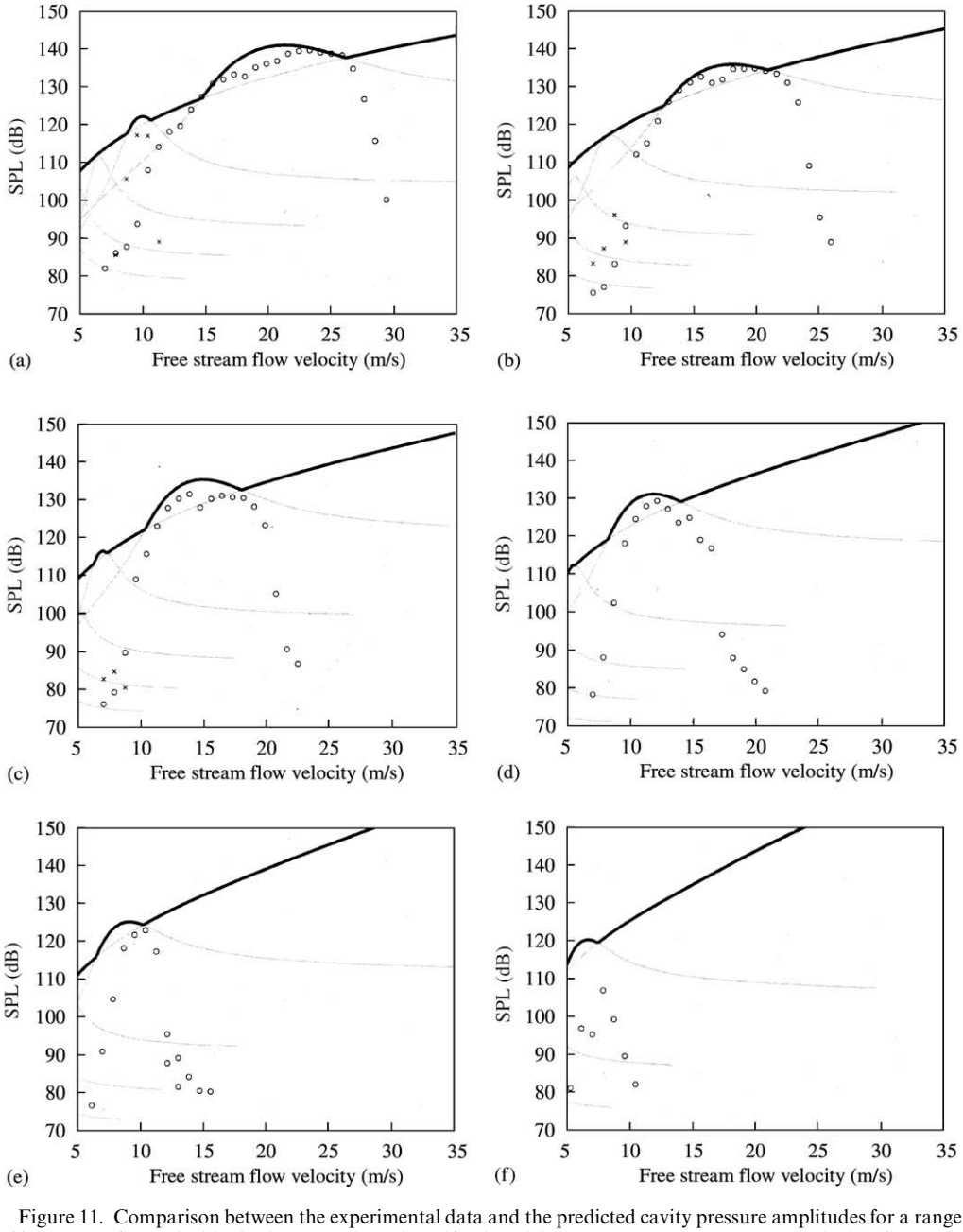


Figure 11. Comparison between the experimental data and the predicted cavity pressure amplitudes for a range of free stream flow velocities in the cases where the orifice length is 8, 7, 6, 5, 4, and 3 cm, respectively, (a)–(f). ○ ○ ○, measured amplitudes associated with the first shear layer excitation mode. X's, measured amplitudes associated with the second shear layer excitation mode. ——, predicted oscillation amplitudes associated with the first and higher shear layer excitation modes. ——, shear layer excitation mode that is predicted to be stable at each free stream flow velocity. (a) $d = 8$ cm; (b) $d = 7$ cm; (c) $d = 6$ cm; (d) $d = 5$ cm; (e) $d = 4$ cm; (f) $d = 3$ cm.

modes are represented by solid lines while darker lines indicate stable limit cycles predicted by the Nyquist stability criterion.

For the cavity pressure oscillation associated with the first shear layer excitation mode, theoretical predictions in both the oscillation frequency and the pressure amplitude are

generally in good agreement with the experimental data over the range of free stream velocities where the first shear layer excitation modes are predicted to be stable. Note that strong self-excited oscillations were initiated near the free stream flow velocities at which the first shear layer excitation mode becomes stable and the self-excited oscillations became quenched near the free stream flow velocities at which the stable mode turns from the first shear layer excitation mode to the shear layer excitation mode zero as shown in Figures 11(a)–11(c). The agreement between the data and the theory for the pressure amplitude predictions, especially in the cases of $d = 4$ and 3 cm as shown in Figures 10(e) and 10(f), respectively, are not as good as for the case of oscillation frequency. However, note that, using the vortex concentration factor (i.e., $\alpha = 0{\cdot}25$) for all orifice lengths, the maximum cavity pressure amplitude was predicted with reasonable accuracy for orifice lengths with the exception of the smallest one, $d = 3$ cm. The Plexiglas inserts used to change the orifice length were placed at the downstream edge of the orifice in the experiments. Thus, it is believed that the decrease in orifice length might have had a negligible influence on the thickness of the incoming shear layer that is also related to the diffusion of vortices.

For the first three orifice lengths ($d = 8$, 7, and 6 cm), the second shear layer excitation mode dominated the first shear layer excitation mode at velocities approximately between 7 to 12 m/s as shown in Figures 11(a)–11(c). The analytical model predicted the oscillation frequencies with a good accuracy, although the second shear layer excitation mode in the case where the orifice length was 7 cm was predicted to be marginally stable. The cavity pressure amplitude associated with the second shear layer excitation mode, however, was overestimated. This may indicate that the energy was not concentrated at the vortical wave number prescribed by the analytical model, but diffused over a wide spectrum of frequencies, making the flow excitation random rather than tonal.

For each orifice length, the lowest shear layer excitation mode (that was referred to as mode zero in section 4.1) was predicted to be stable over specific ranges of free stream flow velocities. For instance, in the case where the orifice length was 8 cm, for stream flow velocities approximately from 5 to 8, 11 to 15, and 26 to 35 m/s, the shear layer excitation mode zero was predicted to be stable as shown in Figures 10(a) and 11(a). However, mode zero was not observed in the experiments. Mode zero is the lowest shear layer excitation mode that is controlled by the cavity feedback (that is, the acoustic flow field near the upstream edge). The wavelength of the vortices associated with such a low shear layer excitation mode would be at least 4 times the cavity orifice length, $d$, off-resonance, and infinitely long at resonance (at which the Strouhal number, $\mathrm{St}_\phi$ approaches zero in theory). However, note that other feedback processes would take over the cavity feedback process for such low frequencies since the shear flow near the upstream edge is sensitive to any small external disturbance, and since such disturbances are very likely to occur (due for example to natural shear layer instabilities). For this reason, it is concluded that mode zero can never be stabilized and no dominant feedback processes exist in the ranges of free stream flow velocities where mode zero is predicted to be stable.

## 6. CONCLUSION

A flow-excited cavity resonator system was analyzed by following a feedback loop approach. A forward gain function required in the feedback loop analysis was developed by using the concept of "vortex sound". Applying vortex sound theory to the modelling of the shear layer's instability yielded a unified procedure to obtain the amplitude gain and the phase lag of the forward gain function. The mathematical procedure allowed the physical

interpretation of many aspects of the flow-excitation mechanism. For example, the external fluctuating force was shown to result from the fluctuation of circulation strength over the orifice and the diffusivity of the vortices over the orifice was shown to affect the amplitude of the excitation force. The validity of the analytical model was verified by showing that the predicted oscillation frequency and the relative amplitude were in reasonably good agreement with the data obtained from experiments performed using a wind tunnel. The usefulness of the feedback loop model was also proven by demonstrating that the stability of the first and the second shear layer modes can be analyzed based on the Nyquist stability criterion.

## ACKNOWLEDGMENTS

The financial support of Ford Motor Company is gratefully acknowledged. Thanks are expressed to Mrs Silvia Zorea, Mr Scott Johnson, and Daniel Brown for their assistance.

## REFERENCES

1. H. KOOK, L. MONGEAU, S. I. ZOREA and D. V. BROWN 1997 *Noise Control Engineering Journal* **45**, 223–234. Analysis of the interior pressure oscillations induced by flow over vehicle openings.
2. J. C. BRUGGEMAN, A. HIRSCHBERG, M. E. H. van DONGEN and A. P. J. WIJNANDS 1991 *Journal of Sound and Vibration* **150**, 371–393. Self-sustained aero-acoustic pulsations in gas transport systems: experimental study of the influence of closed side branches.
3. C. K. W. TAM and P. J. W. BLOCK 1978 *Journal of Fluid Mechanics* **89**, 373–399. On the tones and pressure oscillations induced by flow over rectangular cavities.
4. A. J. BILANIN and E. E. COVERT 1973 *American Institute of Aeronautics and Astronautics Journal* **11**, 347–351. Estimation of possible excitation frequencies for shallow rectangular cavities.
5. D. ROCKWELL 1977 *Journal of Fluids Engineering* **99**, 294–300. Prediction of oscillation frequencies for unstable flow past cavities.
6. M. S. HOWE 1981 *Journal of Fluid Mechanics* **109**, 125–146. The influence of mean shear on unsteady aperture flow, with application to acoustical diffraction and self-sustained cavity oscillations.
7. D. RONNEBERGER 1980 *Journal of Sound and Vibration* **71**, 565–581. The dynamics of shearing flow over a cavity-a visual related to the acoustic impedance of small orifices.
8. W. K. BLAKE 1986 *Mechanics of Flow-Induced Sound and Vibration*. Orlando, FL: Academic Press.
9. M. S. HOWE 1980 *Journal of Sound and Vibration* **70**, 407–411. The dissipation of sound at an edge.
10. A. POWELL 1964 *Journal of the Acoustical Society of America* **36**, 177–195. Theory of vortex sound.
11. L. CREMER and H. ISING 1967 *Acustica* **19**, 143–153. Die selbsterregten schwingungen von orgelpfeifen (in German).
12. S. A. ELDER, 1978 *Journal of the Acoustical Society of America* **64**, 877–890. Self-excited depth-mode resonance for a wall-mounted cavity in turbulent flow.
13. S. A. ELDER, T. M. FARABEE and F. C. DEMETZ 1982 *Journal of the Acoustical Society of America* **72**, 532–549. Mechanisms of flow-excited cavity tones at low mach number.
14. M. MEISSNER 1987 *Acustica* **62**, 220–228. Self-sustained deep cavity oscillations induced by grazing flow.
15. T. D. MAST and A. D. PIERCE 1995 *Journal of the Acoustical Society of America* **97**, 163–172. Describing-function theory for flow excitation of resonators.
16. P. A. NELSON, N. A. HALLIWELL and P. E. DOAK 1981 *Journal of Sound and Vibration* **78**, 15–38. Fluid dynamics of a flow excited resonance. Part I: experiment.
17. P. A. NELSON, N. A. HALLIWELL and P. E. DOAK 1983 *Journal of Sound and Vibration* **91**, 375–402. Fluid dynamics of a flow excited resonance. Part II: flow acoustic interaction.
18. L. E. KINSLER, A. R. FREY, A. B. COPPENS and J. V. SANDERS 1982 *Fundamentals of Acoustics*. New York: John Wiley & Sons.
19. A. GELB and W. E. VAN DER VELDE 1968 *Multiple-Input Describing Functions and Nonlinear System Design*. New York: McGraw-Hill.

20. J. E. ROSSITER 1964 *Aeronautical Research Council Reports and Memoranda No.* 3438. Wind-tunnel experiments on the flow over rectangular cavities at subsonic and transonic speeds.
21. Y. P. TANG and D. ROCKWELL 1983 *Journal of Fluid Mechanics* **126**, 187–204. Instantaneous pressure fields at a corner associated with vortex impingement.
22. H. KOOK 1997 *Ph.D. Thesis, School of Mechanical Engineering, Purdue University*. Prediction and control of the interior pressure fluctuations in a flow-excited Helmholtz resonator.
23. E. E. COVERT 1970 *American Institute of Aeronautics and Astronautics Journal* **8**, 2189–2194. An approximate calculation of the onset velocity of cavity oscillations.
24. J. J. E. SLOTINE and W. LI 1991 *Applied Nonlinear Control*. Englewood Cliffs, NJ: Prentice-Hall.
25. D. V. BROWN and L. MONGEAU 1995 *Ray W. Herrick Laboratories Report No.* 204, *Purdue University*. The design, construction, and validation of a small, low-speed, quiet wind tunnel with application to noise from the flow over a cavity.

## APPENDIX A: NOMENCLATURE

| | |
|---|---|
| $A$ | amplitude of a sinusoidal signal |
| $C_k$ | Fourier series coefficients |
| $d$ | length of the cavity orifice (m) |
| $\mathbf{F}_{ext}$ | force per unit span exerted by convected vortices (N/m) |
| $G(\mathrm{j}\omega)$ | transfer function for the linear part of the system |
| $H$ | amplitude of a rectangular pulse |
| $K_p$ | constant gain of the linear gain function |
| $M$ | equivalent mass of resonator (kg) |
| $N(A, \omega)$ | transfer function for the non-linear part of the system |
| $n_1, n_2, n_3$ | unit vectors along principal axis of co-ordinates |
| $P$ | sound power (W) |
| $p_{ext}$ | external excitation pressure (Pa) |
| $\hat{p}_{ext}$ | phasor of the fundamental component of $p_{ext}$ |
| $\hat{q}_0$ | complex amplitude of the fundamental component of the "excitation" volume velocity ($m^3/s$) |
| $\hat{q}_r$ | complex amplitude of the fundamental component of the "acoustic" volume velocity ($m^3/s$) |
| $(\hat{q}_o/\hat{q}_r)_f$ | forward gain function |
| $(\hat{q}_r/\hat{q}_o)_b$ | backward gain function |
| $S$ | cross-sectional area of a rectangular plane across the region of interest within the orifice (along the $x_1$–$x_2$ plane). |
| $S_o$ | cross-sectional area of the orifice ($m^2$) |
| $\mathrm{St}_\phi$ | Strouhal number, based on the convection velocity, $\mathrm{St}_\phi = \omega d/U_c$ |
| $T$ | period (s) |
| $U_c$ | average vortex convection velocity (m/s) |
| $U_\infty$ | free stream flow velocity (m/s) |
| $\mathbf{u}$ | acoustic velocity vector (m/s) |
| $W$ | rectangular pulse duration (s) |
| $\mathbf{v}$ | total velocity vector (m/s) |
| $v_i$ | total velocity component in the $x_i$ direction (m/s) |
| $\mathbf{v}_v$ | vortical flow velocity vector (m/s) |
| $x_1, x_2, x_3$ | Cartesian co-ordinate system |
| $\alpha$ | vortex concentration parameter |
| $\beta$ | orifice loss factor |
| $\Gamma$ | circulation ($m^2/s$) |
| $\dot{\Gamma}_{in}$ | circulation influx ($m^2/s^2$) |
| $\dot{\Gamma}_{net}$ | rate of change of circulation strength inside a control volume ($m^2/s^2$) |
| $\dot{\Gamma}_{out}$ | circulation outflux ($m^2/s^2$) |
| $\delta_b$ | boundary layer height (m) |
| $\delta(t)$ | Dirac delta function |
| $\rho$ | ambient density ($kg/m^3$) |
| $\tau$ | time delay (s) |
| $\Omega$ | vorticity, $x_3$ component ($s^{-1}$) |

| | |
|---|---|
| $\upsilon$ | control volume over the orifice of the Helmholtz resonator |
| $\omega$ | angular frequency (rad/s) |
| $\omega_r$ | angular resonance frequency (rad/s) |
| $\boldsymbol{\omega}$ | vorticity vector ($s^{-1}$) |
| $\zeta$ | damping ratio |
| $\nabla\phi$ | potential velocity |
| $\hat{[\ ]}$ | denotes a complex variable |
| $\mathbf{[\ ]}$ | denotes a vector |
| $\lvert\ \rvert$ | denotes the magnitude of a complex quantity |
| $\bar{[\ ]}$ | denotes the time average of a time-varying quantity |
| $[\ ]'$ | denotes the unsteady part of a time-varying quantity |